

Physics of star formation history and the luminosity function of galaxies therefrom

Masataka Fukugita¹ and Masahiro Kawasaki²

¹*Kavli Institute for the Physics and Mathematics of the Universe, University of Tokyo, Kashiwa, 277-8583, Japan*

²*Institute for Cosmic Ray Research, University of Tokyo, Kashiwa, 277-8582, Japan*

21 March 2022

ABSTRACT

We show that the star formation history, the reionization history and the present luminosity function of galaxies are reproduced in a simple gravitational collapse model within the Λ CDM regime to almost a quantitative accuracy, when the physical conditions, the Jeans criterion and the cooling process, are taken into account. Taking a reasonable set of the model parameters, the reionisation takes place sharply at around redshift $1 + z \simeq 7.5$, and the resulting luminosity function turns off at $L \simeq 10^{10.7} L_{\odot}$, showing the consistency between the star formation history and the reionisation of the Universe. The model gives the total amount of stars $\Omega_{\text{star}} = 0.004$ in units of the critical density compared to the observation 0.0044 with the recycling factor 1.6 included. In order to account for the observed star formation rate and the present luminosity function, the star formation efficiency is not halo mass independent but becomes maximum at the halo mass $\simeq 10^{12} M_{\odot}$ and is suppressed for both smaller and larger mass haloes.

Key words: galaxies: formation – galaxies: luminosity function – cosmology: reionization

1 INTRODUCTION

Λ CDM model gives the basis of cosmology and the large-scale structure of the universe through gravitational instability of dark matter: the cosmological parameters are precisely determined from the cosmic microwave background (CMB) (Aghanim et al. 2020). Density fluctuations of dark matter grow and collapse into haloes in a hierarchical manner with small haloes produced first and larger haloes formed subsequently merging small halos, as clearly seen in the semi-analytical approach (Press & Schechter 1974; Sheth & Tormen 1999) and also N -body simulations.

Baryons also collapsed in dark matter haloes when gravity overcomes baryonic pressure; they are expected then to cool and form stars. This basic idea for the star formation and the galaxy formation has been developed for years, in e.g. Silk (1977); Rees & Ostriker (1977); Blumenthal et al. (1984). Many papers have appeared using semi-analytic approach (e.g. White & Frenk (1991); Kauffmann et al. (1993); Cole et al. (1994)). Among them Fukugita & Kawasaki (1994); Tegmark et al. (1994); Fukugita & Kawasaki (2003) investigated reionization of the universe by OB stars. Hydrodynamical simulations (Benson et al. 2001; Yoshida et al. 2002; Helly et al. 2003) are employed for investigating the galaxy formation and the large scale structure together with gas dynamics under less assumptions and idealization. The semi-analytic approach, however, has advantage to make underlying physics clear, such as the importance of physical processes involving electrons, baryons and photons that are crucial in formation of stars and galaxies. In large dimensional parameter space large-scale cosmological simulations require a huge

computational cost for varying input parameters. We remark that there are several pieces of the work in this direction, but with different strategies and foci (Trenti et al. 2010; Dekel et al. 2013; Tacchella et al. 2013; Mason et al. 2015; Mirocha et al. 2017; Furlanetto et al. 2017).

In this paper we study the star formation history, as depicted in the ‘Madau plot’ (Madau et al. 1998) and the luminosity function of galaxies using the simple gravitational collapse model in a semi-analytic treatment. The mass function of dark matter haloes is computed using the Press-Schechter approach (Press & Schechter 1974). We apply the cooling and the Jeans conditions to the haloes to obtain star formation: the galaxy haloes are identified when the conditions are satisfied that produce stars. We study the halo mass dependence of the star formation efficiency and calculate evolution of the star formation rate, the reionization history and the luminosity function. We shall observe that the mass dependence is crucial in star formation efficiency f_{eff} for successfully reproducing both observed star formation history and luminosity function.

We note that each individual process has already been studied well in the literature to now. What we are going to do is ‘engineering’, putting together the processes and to find if this would produce the observation correctly, and what conditions are needed. It is important that we can study the dependence on the input parameters. Compared with similar studies (Trenti et al. 2010; Dekel et al. 2013; Tacchella et al. 2013; Mason et al. 2015; Mirocha et al. 2017; Furlanetto et al. 2017) our focus is on the star formation history and the luminosity function along with the ionisation history. In our

calculation the luminosity-mass relations of main-sequence and red giant stars are used as input.

In Sec. 2 the formulae are assembled to calculate the star formation rate and the luminosity function. In Sec. 3 we present the star formation history, the reionization history and the luminosity function of galaxies. Sec. 4 presents the conclusion we obtained. In this paper we take Λ CDM model with the cosmological parameters

$$\begin{aligned} h = 0.673 & & \Omega_m h^2 = 0.143 & & \Omega_b h^2 = 0.0224 \\ n_s = 0.965 & & \sigma_8 = 0.811 & & Y_p = 0.247 \end{aligned} \quad (1)$$

for the Hubble constant, the total matter density, the baryon density, the spectral index, the fluctuation amplitude at $8h^{-1}$ Mpc, and the helium abundance, as taken from Planck 2018 (Aghanim et al. 2020).

2 SIMPLE GRAVITATIONAL COLLAPSE MODEL

2.1 Basic formulae used

The halo mass function may be calculated with the Press-Schechter formula (Press & Schechter 1974). Here we adopt a more accurate fitting formula by Sheth and Tormen (Sheth & Tormen 1999). The halo comoving number density $N(M, z)$ with mass $M \sim M + dM$ is written as

$$n(M, z) = A \sqrt{\frac{2}{\pi}} \frac{\rho_{m0}}{M} \left(\frac{a\delta_c^2}{\sigma(M)^2} \right)^{1/2} \left(1 + \left(\frac{a\delta_c}{\sigma(M)^2} \right)^{-p} \right) \left| \frac{\partial \ln \sigma(M)}{\partial M} \right| \exp \left(-\frac{a\delta_c^2}{2\sigma(M)^2} \right), \quad (2)$$

where ρ_{m0} is the present matter density, $\delta_c = 1.686$, $a = 0.707$, $p = 0.3$, $A = 0.322$ and $\sigma(M)$ is the coarse-grained variance. In working details we follow the formalism of Bardeen et al. (1986).

Baryons collapse in dark matter haloes, if the gravity overcomes the baryon pressure, namely if the halo mass is larger than the Jeans mass M_J ,

$$M_J = 1.4 \times 10^4 M_\odot (\Omega_m h^2)^{-1/2} \left(\frac{T_e}{\mu T} \right)^{3/2}, \quad (3)$$

where T is the cosmic temperature, T_e the electron temperature, and μ the mean molecular weight.

Star formation takes place when baryons lose their energy through atomic and molecular cooling. The atomic cooling of hydrogen and helium becomes effective when the virial temperature T_{vir} is larger than about 10^4 K, where

$$T_{\text{vir}} = 0.01 \text{ K} \left(\frac{M}{M_\odot} \right)^{2/3} \mu (1+z) (\Omega_m h^2)^{1/3} \left(\frac{\rho/\bar{\rho}}{178} \right)^{1/3}, \quad (4)$$

with $\rho(\bar{\rho})$ the halo (background) density. Eq. (4) indicates that the atomic cooling works if

$$M > M_{\text{ac}} = 2.1 \times 10^9 M_\odot (\Omega_m h^2)^{-1/2} (1+z)^{-3/2}. \quad (5)$$

Here we take $\mu = 1.22$ and $\rho/\bar{\rho} = 178$. The molecular cooling condition (Blumenthal et al. 1984) is

$$M > M_{\text{mc}} = 2.1 \times 10^8 M_\odot (\Omega_m h^2)^{-0.917} \times \left(\frac{Y_e}{10^{-4}} \right)^{-0.625} \left(\frac{\Omega_b}{\Omega_m} \right)^{-2.04} (1+z)^{-2.75}, \quad (6)$$

where Y_e is the fraction of free electrons.

For large haloes with virial temperature $T_{\text{vir}} \gtrsim 10^6$ K, the cooling rate is also controlled by metal cooling or Compton cooling. The metal cooling rate (Dalgarno & McCray 1972) is given by

$$\Lambda_{\text{metal}} \simeq 1.45 \times 10^{-7} \left(\frac{Z}{Z_\odot} \right) \text{ K cm}^3 \text{ s}^{-1} \quad (T \gtrsim 10^6 \text{ K}), \quad (7)$$

with $Z(Z_\odot)$ the (solar) metallicity. For efficient cooling in haloes, $T_{\text{vir}}/(n_B \Lambda_{\text{metal}}) \lesssim H^{-1}$, which leads to

$$M < M_{\text{metal}} = 3.0 \times 10^{14} M_\odot (\Omega_b h^2)^{3/2} (\Omega_m h^2)^{5/4} \left(\frac{Z}{0.01} \right)^{3/2}. \quad (8)$$

On the other hand, Compton cooling is efficient if

$$1+z \gtrsim 1+z_{\text{comp}} = 5.3 \left(\frac{\Omega_m h^2}{0.25} \right)^{1/5}. \quad (9)$$

Thus, we assume that star formation starts if the halo mass M satisfies

$$M_{\text{min}} < M < M_{\text{max}}, \quad (10)$$

where

$$M_{\text{min}} = \max[M_J, \min(M_{\text{ac}}, M_{\text{mc}})] \quad (11)$$

$$M_{\text{max}} = \begin{cases} M_{\text{metal}} & (z < z_{\text{comp}}) \\ \infty & (z > z_{\text{comp}}) \end{cases}. \quad (12)$$

In calculating the star formation we assume that the formation rate is proportional to the derivative of the halo mass function, $\partial n(M, t)/\partial t$ which is considered as the formation rate of halos with mass M . In the Press-Schechter theory, halos are formed through accretion and merger. Thus, $\partial n(M, t)/\partial t$ is proportional to the rate of accretion into halos when the accretion is the dominant process.¹ In this paper, we neglect the effect of the merger.

We assume that stars are produced in two ways: the burst star formation takes place when the haloes formed with the rate

$$\psi_b(z) = \int_{M_{\text{min}}}^{M_{\text{max}}} dM F_b f_{\text{eff}}(M) \frac{\Omega_b}{\Omega_m} M \frac{\partial n(M, z)}{\partial t}, \quad (13)$$

where F_b is the maximum fraction of collapsed baryons that form stars in a burst and $f_{\text{eff}} F_b$ is the efficiency of star formation which may depend on the halo mass M . With the baryons survived the burst stars formed continuously in haloes. We assume that stars form at a constant rate per baryon mass for the duration τ_c . The star formation rate is then written

$$\psi_c(z) = \int_{t(z)-\tau_c}^{t(z)} dt' \int_{M_{\text{min}}}^{M_{\text{max}}} dM \frac{\Omega_b}{\Omega_m} \dot{F}_c f_{\text{eff}}(M) \frac{\partial n(M, z(t'))}{\partial t'}, \quad (14)$$

where \dot{F}_c is the maximum star formation rate per baryonic mass in a halo. The observation suggests that star formation

¹ If we consider accretion only, the halo mass function evolves as $N(M, t) = N(M - \dot{M}dt, t - dt)$, which leads to $\partial N/\partial t = \dot{M}(-\partial N/\partial M)$. Here \dot{M} is the accretion rate of dark matter into a halo with mass M .

is less efficient for low mass galaxies. Massive galaxies with $M \gtrsim 10^{13} M_\odot$ are rare too. In order to take account of these suppressions, we introduce the star forming efficiency f_{eff} , assuming that it depends on the halo mass, as

$$f_{\text{eff}} = \begin{cases} (M/M_*)^{\alpha_L} & \text{for } M \leq M_* \\ (M/M_*)^{-\alpha_H} & \text{for } M > M_*, \end{cases} \quad (15)$$

where we take $M_* = 10^{12} M_\odot$; we also take a default $\alpha_L \sim 0.7$ and $\alpha_H \sim 1$, as discuss below. The total star formation rate ψ_{sfr} is given by the sum

$$\psi_{\text{sfr}} = \psi_b + \psi_c. \quad (16)$$

2.2 UV photons

The UV photons emitted from stars with mass larger than $\sim 10 M_\odot$ reionize the universe and heat the intergalactic medium, which then affects star formation through the modification of the Jeans mass. We adopt the [Chabrier \(2003\)](#) initial mass function (IMF)

$$\log_{10} \phi(m_s) = \begin{cases} A - 0.912 \log_{10}(m_s/M_\odot) \\ -0.456 [\log_{10}(m_s/M_\odot)]^2 & (m_s < 1 M_\odot), \\ A - 1.3 \log_{10}(m_s/M_\odot) & (m_s \geq 1 M_\odot), \end{cases} \quad (17)$$

where m_s is the mass of stars. A is the normalisation so that $\int dm_s \phi(m_s) = 1$. The stellar temperature-mass relation for Population II ($Z < 0.001$) and I ($Z > 0.01$) stars is given by ([Bond et al. 1986](#))

$$T_s(m_s) = \begin{cases} 6 \times 10^4 \text{ K} \min \left[\left(\frac{m_s}{100 M_\odot} \right)^{0.3}, 1 \right] & (Z < 0.001) \\ 4.3 \times 10^4 \text{ K} \min \left[\left(\frac{m_s}{100 M_\odot} \right)^{0.3}, 1 \right] & (Z > 0.01), \end{cases} \quad (18)$$

respectively. For $0.001 < Z < 0.01$ we consider a mixture of two populations with the Population I fraction ($Z - 0.001$)/0.009.

Lifetime of stars with $m_s \gtrsim 10 M_\odot$ that emits ionising UV is shorter than 10^8 yr, shorter than the Hubble time at $z < 20$. Therefore, we may assume that UV photons are emitted instantaneously upon the formation of stars. UV photons with energy ε_γ are produced, as

$$\frac{dn_\gamma(\varepsilon_\gamma, z)}{dt} = f_{\text{esc}} \int dm_s \frac{B(\varepsilon_\gamma, T_s)}{\varepsilon_\gamma} \epsilon_s \phi(m_s) \frac{\Omega_b}{\Omega_m} \psi_{\text{sfr}}(z), \quad (19)$$

where $B(\varepsilon_\gamma, T_s)$ is the blackbody spectrum normalized as $\int d\varepsilon_\gamma B(\varepsilon_\gamma) = 1$, and ϵ_s is the fraction of the radiation energy to the rest mass.

Here, we introduce the escape fraction f_{esc} to account for absorption of UV photons while escaping the halo. We follow the evolution of the UV photon spectrum $n_\gamma(\varepsilon_\gamma)$ by numerically integrating the Boltzmann equation with source term given by Eq. (19). We calculate the cumulative effective ionizing flux,

$$F_{\text{ion}}(z) = \int_{\varepsilon_{\text{th}}}^{\infty} d\varepsilon_\gamma \frac{\sigma_{\text{ph}}(\varepsilon_\gamma)}{\sigma_{\text{ph}}(\varepsilon_{\text{Th}})} \int^t dt' \frac{dn_\gamma(\varepsilon_\gamma(1+z')/(1+z), z')}{dt'}, \quad (20)$$

where σ_{ph} is the photoionization cross section of hydrogen and $\varepsilon_{\text{th}} = 13.6$ eV.

We calculate the evolution of the electron temperature taking into account photoionization, collisional ionization, Compton heating and cooling, also including other minor processes as detailed in [Fukugita & Kawasaki \(1994\)](#). Furthermore, we solve the evolution equation for fractions of HI, HII, HeI, HeII, and HeIII.

We follow the evolution of metallicity. Stars with mass $m_s > 4 M_\odot$ produce heavy elements at a fraction ([Carr et al. 1984](#))

$$Z_{\text{ej}} = \begin{cases} 0.5 - (m_s/6.3 M_\odot)^{-1} & (15 < m_s/M_\odot < 100) \\ 0.1 & (8 < m_s/M_\odot < 15) \\ 0.2 & (4 < m_s/M_\odot < 8). \end{cases} \quad (21)$$

The evolution of metallicity is

$$\frac{dZ}{dt} = \frac{1}{\rho_{\text{b0}}} \int dm_s Z_{\text{ej}} \phi(m_s) \psi_{\text{sfr}}(z). \quad (22)$$

2.3 Luminosity function

For the luminosity function of galaxies long-lived stars with mass $m_s \lesssim 10 M_\odot$ are important. We adopt the luminosity-mass relation of the main-sequence stars in [Reid et al. \(2002\)](#), where the stellar mass is translated to luminosity and represented as absolute magnitude. We obtain the inverse relation, magnitude as a function of stellar mass, as

$$M_V - M_{V\odot} = -13.463 x + 0.823 x^2 + 5.920 x^3 - 0.570 x^4 + 1.232 x^5, \quad (23)$$

where $x = \log_{10}(m_s/M_\odot)$, M_V is the absolute magnitude for the V-band luminosity, $L_{\text{MS}} = 10^{-0.4(M_V - M_{V\odot})} L_\odot$. Here we consider only stars with mass less than $10 M_\odot$, whose main sequence time is given by

$$\log_{10}(t_{\text{MS}}/\text{yr}) = 10.03 - 3.45 x + 0.786 x^2 \quad (m_s < 10 M_\odot) \quad (24)$$

For low mass stars with $m_s < 2 M_\odot$ the time spent in the red giant phase is significant compared to t_{MS} . The red giant branch time t_{RGB} ([Serenelli & Fukugita 2007](#)) may be fitted as

$$\log_{10}(t_{\text{RGB}}/\text{yr}) = 9.514 - 3.907 x - 19.50 x^2 + 43.60 x^3 \quad (m_s < 2 M_\odot), \quad (25)$$

and luminosity of stars in the red giant branch is

$$\log_{10}(L_{\text{RGB}}/L_{\text{MS}}) = 8.63 - 18.4 (m_s/M_\odot) + 14.2 (m_s/M_\odot)^2 - 3.51 (m_s/M_\odot)^3. \quad (26)$$

The luminosity to mass ratio L/M of the galaxy formed at t_f is written

$$\begin{aligned} \left(\frac{L}{M}\right)(t, t_f) = & F_b \frac{\Omega_b}{\Omega_m} \left[\int^{10M_\odot} dm_s \theta[t_{\text{MS}}(m_s) - (t - t_f)] L_{\text{MS}}(m_s) \phi(m_s) \right. \\ & + \int^{2M_\odot} dm_s \theta[t_{\text{MS}}(m_s) + t_{\text{RGB}}(m_s) - (t - t_f)] \\ & \left. \times \theta[(t - t_f) - t_{\text{MS}}(m_s)] L_{\text{RGB}}(m_s) \phi(m_s) \right] \\ & + \dot{F}_c \frac{\Omega_b}{\Omega_m} \int_{t_f}^{\min(t, t_f + \tau_c)} dt' \\ & \left[\int^{10M_\odot} dm_s \theta[t_{\text{MS}}(m_s) - (t - t')] L_{\text{MS}}(m_s) \phi(m_s) \right. \\ & + \int^{2M_\odot} dm_s \theta[t_{\text{MS}}(m_s) + t_{\text{RGB}}(m_s) - (t - t')] \\ & \left. \times \theta[(t - t') - t_{\text{MS}}(m_s)] L_{\text{RGB}}(m_s) \phi(m_s) \right]. \end{aligned} \quad (27)$$

The luminosity function is

$$\Phi(L, z) = \int^{t(z)} dt' \int dM \left(\frac{L}{M}\right)(t, t') M \frac{\partial n(M, z(t'))}{\partial t'}. \quad (28)$$

Note that $\left(\frac{L}{M}\right)(t, t_f)$ is a decreasing function of t ; massive stars ($m_s > 2M_\odot$) with the main-sequence time shorter than $t - t_{\text{sf}}$ (t_{sf} : star formation time) do not contribute to luminosity.

3 RESULTS

Our calculation contains 7 model parameters ($\alpha_{\text{H}}, \alpha_{\text{L}}, M_*, F_b, \dot{F}_c, \tau_c, f_{\text{esc}}$). The stellar mass function of galaxies (Bernardi et al. 2013; Wright et al. 2017) turns off at around $M_* \sim (10^{11} - 10^{12})M_\odot$. For low masses $M < M_*$ it is indicated that the mass function is suppressed by a factor $M^{-0.4} - M^{-0.7}$ relative to the mass function of dark matter (Bullock & Boylan-Kolchin 2017). For galaxies $\gtrsim 10^{11}M_\odot$, on the other hand, the suppression of the stellar mass function is given approximately by $\alpha_{\text{H}} \sim 1.0$ (Bullock & Boylan-Kolchin 2017) relative to dark matter. Here we remark that, unlike the suppression factor in Bullock & Boylan-Kolchin (2017), our $\alpha_{\text{H(L)}}$ does not include suppression of star formation coming from the cooling and the Jeans conditions, which may lead to smaller $\alpha_{\text{H(L)}}$.

We take the fraction of the burst formation of stars to be 0.4 to fit the star formation rate history better, which is somewhat larger than that implied by the age distribution of the stars in the solar neighborhood (Barry 1988), which suggests (burst):(continuous) = $F_b : \dot{F}_c \tau_c \sim 0.3 : 0.7$.² We take the duration of the star formation as $\tau_c \sim 10$ Gyr. The escape fraction f_{esc} was measured by a number of authors, e.g., in Leitherer et al. (1995); Hurwitz et al. (1997); Heckman

² Here we take stars with age less than 2.5 Gyr after the onset of collapse as formed in the burst.

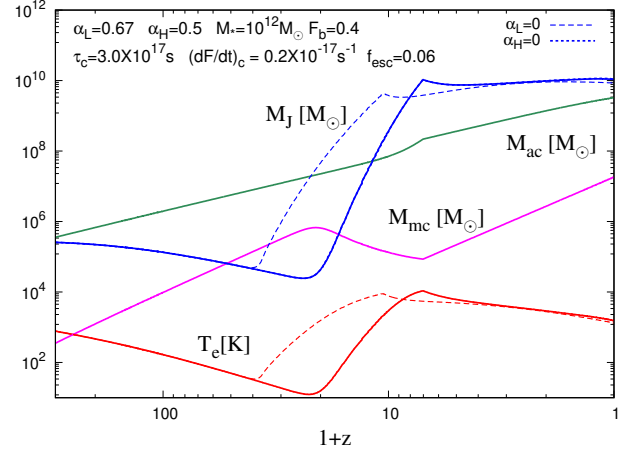


Figure 1. Evolution of the Jeans mass (blue), the lower bound from atomic cooling (green), the lower bound from atomic cooling (magenta), and of the electron temperature (red). The Jeans mass and the electron temperature for $\alpha_{\text{L}} = 0$ or $\alpha_{\text{H}} = 0$ are also shown by dashed or dotted lines. The dotted lines may not be discernible as they almost degenerate with the curves for the default.

et al. (2001); Bouwens et al. (2015b) [see also, Robertson et al. (2015); Sun & Furlanetto (2016)], which vary but give typically $f_{\text{esc}} \approx 0.03 - 0.1$.

From these observational implications and a comparison of our calculation with the star formation and reionization histories and with the galaxy luminosity function (which we show below), we take

$$\begin{aligned} \alpha_{\text{L}} = 0.67, \quad \alpha_{\text{H}} = 0.5, \quad M_* = 10^{12} M_\odot, \quad F_b = 0.4 \\ \tau_c = 3 \times 10^{17} \text{ s}, \quad \dot{F}_c = 0.2 \times 10^{-17} \text{ s}^{-1}, \quad f_{\text{esc}} = 0.06 \end{aligned} \quad (29)$$

as our optimal default set of the model parameters.

3.1 Star formation rate

The minimum halo mass for star formation is determined by the Jeans and cooling criteria (3)-(6), which are depicted in Fig. 1. We see that the Jeans mass gives the lower bound for star formation at $z \lesssim 10$, while the molecular cooling condition gives the minimum mass for $10 \lesssim z \lesssim 50$. By $z \lesssim 6$ the Jeans mass rapidly increases to $\simeq 10^{10}M_\odot$, which strongly suppresses the formation of star forming galaxies. This rapid rise is caused by the increase of the electron temperature due to heating with UV photons emitted from early galaxies.

We also include in this figure the evolution of the Jeans mass and electron temperature for $\alpha_{\text{L}} = 0$ or $\alpha_{\text{H}} = 0$ by dashed or dotted lines, respectively. The dotted lines for $\alpha_{\text{H}} = 0$ are barely discernible from the default curve. For $\alpha_{\text{L}} = 0$, on the other hand, the electron temperature and Jeans mass increase earlier, since a large number of stars are produced in early-formed low-mass haloes without the suppression of the star formation efficiency (see Fig. 2). For $\alpha_{\text{H}} = 0$ the star formation is enhanced close to the present epoch, too large for $z \lesssim 0.3$. This, however, hardly changes the electron temperature, because the hydrogen is already fully ionized so that the energy deposition by UV photons from stars is small.

The cosmic star formation rate for our default model pa-

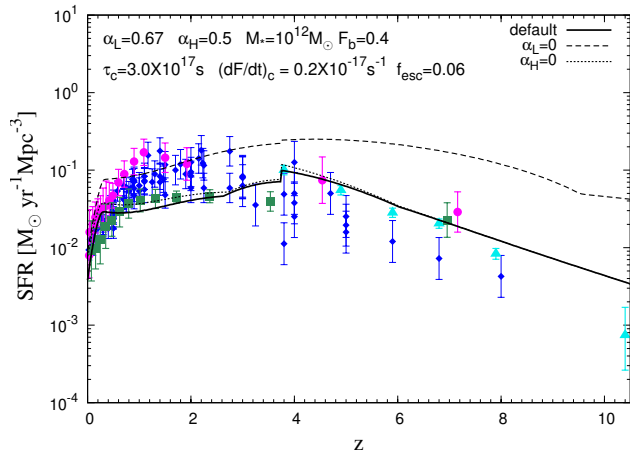


Figure 2. Cosmic star formation rate (solid line) compared with the observation (Behroozi et al. 2013b) (blue points), (Bouwens et al. 2015a) (cyan points), (Sánchez et al. 2019) (magenta points) and (López Fernández et al. 2018) (green points). The star formation rate with the formation efficiency $(\alpha_L, \alpha_H) = (0, 1.4)$ and $(0.7, 0)$ are shown with dashed and dotted lines, respectively.

rameters is shown with solid line in Fig. 2. This is compared with the recent compilation of observations (Behroozi et al. 2013b), which are shown in blue points in the figure. Since our cosmic star formation rate is calculated without the luminosity cutoff, it overproduces the star formation rate compared to the observed data at high redshifts. The estimated star formation rate history is consistent with the observation within error bars.

The small kink of the curve seen at $z \sim 4$ is due to the Compton cooling that decouples at this epoch, which changes M_{max} rapidly as seen in Eq. (12). This effect, however, is not important, because few large halos formed at a high redshift. The star formation rate shows a rapid decrease around $z \sim 0.3$. This comes from our choice of the star formation duration τ_c , or $t_0 - \tau_c$ which corresponds to $z \sim 0.3$. The star formation ceases in galaxies formed early, which accounts for the rapid decrease of the star formation rate, consistent with the decrease seen in what is observed. In other words, the duration of the star formation $\tau_c \simeq 10$ Gyr is required from comparison with the observation.

The efficiency for star formation that depends on the halo mass is represented by the parameters α_L and α_H , as in Eq. (15). If we would assume a mass independence of the efficiency, i.e. $\alpha_L = 0$, for low mass halos, the resulting star formation rate becomes much too large at $z \gtrsim 3$ as seen in Fig. 2; without suppression of the formation efficiency too much more stars are produced in small halos. On the other hand, for $\alpha_H = 0$ the estimated star formation rate differs little from the default case.

3.2 Reionization history

The UV flux from stars (19) heats the background plasma and ionizes hydrogen and helium in the intergalactic medium. We calculate the reionization history and the evolution of the electron temperature.

Fig. 3 shows the reionization history. The blue and red

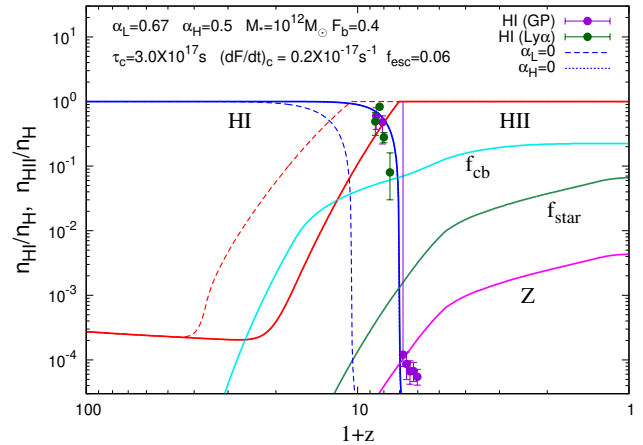


Figure 3. Fractions of HI (blue) and HII (red) against total hydrogen. Filled circles show the volume-averaged neutral fraction from the Gunn-Peterson test (Fan et al. 2006; Davies et al. 2018) (violet) and Ly α emission (Jung et al. 2020; Morales et al. 2021) (green). The evolution of HI and HII for $\alpha_L = 0$ or $\alpha_H = 0$ is shown by dashed or dotted lines. The evolution of metallicity Z (magenta), the fraction f_{star} of baryons used for star formation (green) and the fraction f_{cb} of cooled baryons that could be used to form stars are also shown (light blue line).

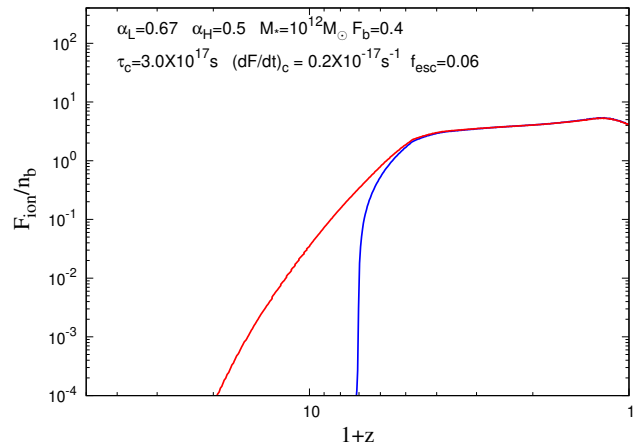


Figure 4. Ratio of the effective ionizing flux to the baryon number density. The red (blue) solid line represents the cumulative value without (with) absorption by the intergalactic medium.

solid lines denote the fraction of HI and HII, respectively. The observed HI fraction from measurements of the Gunn-Peterson optical depth (Fan et al. 2006; Davies et al. 2018) and Lyman-alpha emission (Jung et al. 2020; Morales et al. 2021) is also shown. The model shows that the HI fraction ($\sim 70\%$) at $z \sim 7$ is larger than the observation from the Lyman-alpha emission. On the other hand, the recent observation of the mean free path of ionising photons (Becker et al. 2021) implies that the HI fraction is larger than 20% at $z = 6$. The uncertainty is still significant in the observed HI fraction around these redshifts. We note that in a highly dense region UV flux may be screened and HI remains to lower redshift. This is not taken into account in our calculation. We also

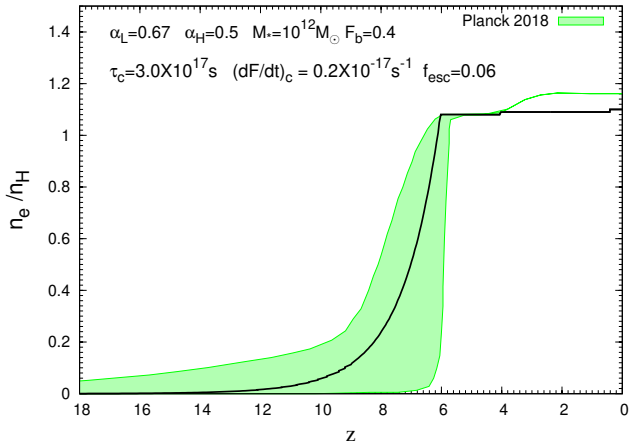


Figure 5. Evolution of the free electron fraction (black line) with respect to the hydrogen amount compared with the constraint from Plank (green region) (Aghanim et al. 2020).

show the evolution of the cumulative ionising flux (20), emitted and after absorbed by IGM, in Fig. 4 below.

In Figs. 3 we see that reionization takes place around $z \simeq 6.5$ when the ionization flux reaches a fraction (0.2–0.3) of the baryon number density (Fig. 4). The resulting reionization epoch agrees with the observed optical depth in QSO lights (Fan et al. 2006; Davies et al. 2018).

The reionization history for $\alpha_L = 0$ or $\alpha_H = 0$ is also depicted by dashed or dotted lines. With $\alpha_H = 0$ the electron temperature raised earlier as in Fig. 1, the ionization fraction of the hydrogen increases earlier, and the reionization takes place around $z \simeq 10$. On the other hand, with $\alpha_L = 0$ the increase of star formation efficiency for large haloes hardly affects the reionization history; the line is basically degenerate with the default curve.

With this reionization history we calculate the optical depth $\tau = 0.051$, which agrees with the Planck 2018 value, $\tau = 0.054 \pm 0.007$ (Aghanim et al. 2020). Fig.5 shows the evolution of the free electron fraction compared with that constrained from the Planck observation (Fig.45 of Aghanim et al. (2020)). The free electron fraction derived from the Planck data show some increase at $z = 3.5$ towards lower redshift. This is because the Planck analysis assumes the full ionization of helium at $z \lesssim 3.5$, which gives a negligible contribution to τ . Taking this into account, the free electron fraction is in a good agreement with the Plank observation.

In Fig. 3 we also plot the evolution of metallicity (Z), the fraction of baryons that have experienced star formation (f_{star}), and the fraction of the cooled baryons against the total (f_{cb}). We see that stars are about 1/4 the baryons that satisfy the cooling conditions. Star formation starts around $z \gtrsim 10$. A significant fraction of stars ($\sim 40\%$) formed between $z = 1$ and $z = 3$. The final fraction of stars amounts to $f_{\text{star}} \simeq 0.07$, or $\Omega_{\text{star}} \simeq 0.004$. In Fukugita & Peebles (2004) it is estimated that fraction of baryons that undergo stars is $\Omega_{\text{star}} = 0.0027 \times 1.62 = 0.0044$, where the first number is the present day mass density of stars, and the second is a correction for recycling. The metallicity evolves in a similar way and the global mean of present-day metallicity is $Z \simeq 0.005$.

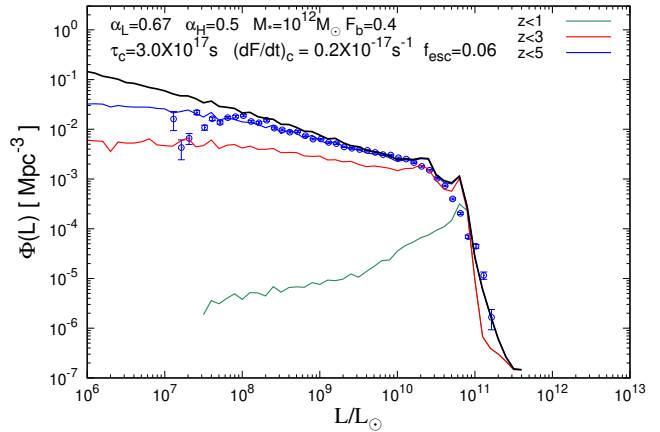


Figure 6. Present-day luminosity function of galaxies (black line). We indicate the luminosity functions of halos formed at $z < 5$ (blue), $z < 3$ (red) and $z < 1$ (green). The data points are taken from the SDSS observation of Blanton et al. (2005).

3.3 Luminosity function

In Fig. 6 we show the present-day luminosity function of galaxies with thick black line using Eq. (28). We show the SDSS observation (Blanton et al. 2005) with data points. How much haloes formed at $z < 5$, $z < 3$ and $z < 1$ contribute to the present-day luminosity function are also indicated. The derived luminosity function (black line) is broadly consistent with the observation, including the overall normalization (up to a factor of < 2) and the turn off of the luminosity function. It is found that most contribution comes from galaxies formed between $z = 5$ and $z = 1$. A significant fraction of low luminosity galaxies with $L \lesssim 10^9 L_\odot$ still form at $5 > z > 3$.

In Fig. 7 we show, for comparison, the luminosity function for different star formation efficiencies, in addition to our default choice $(\alpha_L, \alpha_H) = (0.67, 0.5)$, the two cases with more formation in earlier (0, 0.5) or later epoch (0.67, 0). For $\alpha_L = 0$ the luminosity function becomes too large, especially at low luminosity. On the other hand, if we take $\alpha_H = 0$, the model gives too large a number of high luminosity galaxies, the turn-off luminosity largely shifted to a brighter side. The agreement with the observation is achieved only by introducing suppression factors in the star formation rate in both high and low mass haloes.

The compatibility of both star formation rate and luminosity function with the observation mean that the star formation efficiency should have a peak around $M_* = 10^{12} M_\odot$ and suppressed for both $M < M_*$ and $M > M_*$. Our choice $\alpha_L = 0.67$ and M_* agree with Behroozi et al. (2013a) who give $\alpha_L \sim 2/3$ and $\alpha_H \sim 4/3$ with $M_* \simeq 10^{11.7} M_\odot$. On the other hand, our model shows a weaker suppression for $M > M_*$. This is due to the fact that the ineffective metal cooling suppresses the star formation in addition to the factor of $(M/M_*)^{-\alpha_H}$, which makes our α_H smaller than that in Behroozi et al. (2013a).

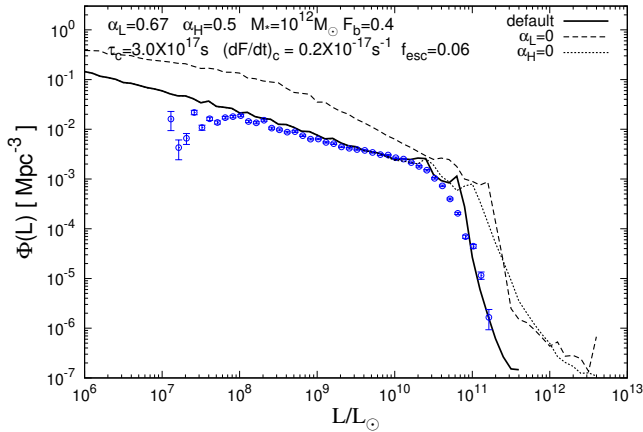


Figure 7. Present-day luminosity functions for $(\alpha_L, \alpha_H) = (0.7, 1.4)$ (solid), $(0, 1.4)$ (dashed) and $(0.7, 0)$ (dotted).

4 CONCLUSION

We have studied the reionization history, star formation history, and the present luminosity function of galaxies using the simplest model of galaxy formation in Λ CDM cosmology. We have found that the simple semi-analytic model, a la Press and Schecheter (1974), can account for the observed reionization epoch, the star formation rate and the present-day luminosity function to almost a quantitative accuracy, if the physical processes, the Jeans condition and the cooling conditions are properly taken into account. The total amount of stars formed are estimated to be $\Omega_{\text{star}} = 0.004$ compared to the observation 0.0044 including the recycling factor. The epoch of reionisation is estimated to occur sharply at $1 + z \simeq 7.5$.

To account for the observed time dependence of the star formation rate and for the present luminosity function of galaxies, both independently requires that the star formation efficiency should increase with the halo mass for $M < M_*$, it reaches a maximum at the turn-off mass of $M_* \sim 10^{12} M_\odot$, and then it should decrease towards larger halo mass. Namely, there is an optimal mass for star formation, $M \sim 10^{12} M_\odot$ for the halo mass, or $M \sim 10^{10} M_\odot$ for the stellar mass of galaxies. This is the only constraints to be added to the model of the collapse.

Our simple model accounts for the observed star formation history and the present-day luminosity function by choosing appropriately a set of 7 parameters. Among them f_{esc} , F_b and $\bar{F}_c \tau_c$ are taken consistently with the direct observations of the escape fraction and the age distribution of the stars in the solar neighborhood. The three more parameters that control the mass-dependent star formation rate, α_H , α_L , and M_* , are determined to make the result consistent with the observation.

ACKNOWLEDGEMENTS

This work was supported by JSPS KAKENHI Grant Nos. 20H05851(M.K.), 21K03567(M.K.), and World Premier International Research Center Initiative (WPI Initiative), MEXT, Japan (M.F, M.K.).

DATA AVAILABILITY

No new data were generated or analysed in this article. The code that we developed to produce the results presented in this manuscript is undergoing further extension, and we plan to publicly release it at a later stage as part of a follow-up work.

REFERENCES

- Aghanim N., et al., 2020, *Astron. Astrophys.*, 641, A6
 Bardeen J. M., Bond J. R., Kaiser N., Szalay A. S., 1986, *Astrophys. J.*, 304, 15
 Barry D. C., 1988, *Astrophys. J.*, 334, 436
 Becker G. D., D’Aloisio A., Christenson H. M., Zhu Y., Worseck G., Bolton J. S., 2021, *Mon. Not. Roy. Astron. Soc.*, 508, 1853
 Behroozi P. S., Wechsler R. H., Conroy C., 2013a, *Astrophys. J. Lett.*, 762, L31
 Behroozi P. S., Wechsler R. H., Conroy C., 2013b, *Astrophys. J.*, 770, 57
 Benson A. J., Pearce F. R., Frenk C. S., Baugh C. M., Jenkins A., 2001, *Mon. Not. Roy. Astron. Soc.*, 320, 261
 Bernardi M., Meert A., Sheth R. K., Vikram V., Huertas-Company M., Mei S., Shankar F., 2013, *Mon. Not. Roy. Astron. Soc.*, 436, 697
 Blanton M. R., Lupton R. H., Schlegel D. J., Strauss M. A., Brinkmann J., Fukugita M., Loveday J., 2005, *Astrophys. J.*, 631, 208
 Blumenthal G. R., Faber S. M., Primack J. R., Rees M. J., 1984, *Nature*, 311, 517
 Bond J. R., Carr B. J., Hogan C. J., 1986, *Astrophys. J.*, 306, 428
 Bouwens R. J., et al., 2015a, *Astrophys. J.*, 803, 34
 Bouwens R. J., Illingworth G. D., Oesch P. A., Caruana J., Holwerda B., Smit R., Wilkins S., 2015b, *Astrophys. J.*, 811, 140
 Bullock J. S., Boylan-Kolchin M., 2017, *Ann. Rev. Astron. Astrophys.*, 55, 343
 Carr B. J., Bond J. R., Arnett W. D., 1984, *Astrophys. J.*, 277, 445
 Chabrier G., 2003, *Publ. Astron. Soc. Pac.*, 115, 763
 Cole S., Aragon-Salamanca A., Frenk C. S., Navarro J. F., Zepf S. E., 1994, *Mon. Not. Roy. Astron. Soc.*, 271, 781
 Dalgarno A., McCray R. A., 1972, *Ann. Rev. Astron. Astrophys.*, 10, 375
 Davies F. B., et al., 2018, *Astrophys. J.*, 864, 142
 Dekel A., Zolotov A., Tweed D., Cacciato M., Ceverino D., Primack J. R., 2013, *Mon. Not. Roy. Astron. Soc.*, 435, 999
 Fan X.-H., et al., 2006, *Astron. J.*, 132, 117
 Fukugita M., Kawasaki M., 1994, *Mon. Not. Roy. Astron. Soc.*, 269, 563
 Fukugita M., Kawasaki M., 2003, *Mon. Not. Roy. Astron. Soc.*, 343, L25
 Fukugita M., Peebles P. J. E., 2004, *Astrophys. J.*, 616, 643
 Furlanetto S. R., Mirocha J., Mebane R. H., Sun G., 2017, *MNRAS*, 472, 1576
 Heckman T., Sembach K. R., Meurer G., Leitherer C., Calzetti D., Martin C. L., 2001, *Astrophys. J.*, 558, 56
 Helly J. C., Cole S., Frenk C. S., Baugh C. M., Benson A., Lacey C. G., Pearce F. R., 2003, *Mon. Not. Roy. Astron. Soc.*, 338, 913
 Hurwitz M., Jelinsky P., Dixon W. V. D., 1997, *Astrophys. J. Lett.*, 481, L31
 Jung I., et al., 2020, *ApJ*, 904, 144
 Kauffmann G., White S. D. M., Guiderdoni B., 1993, *Mon. Not. Roy. Astron. Soc.*, 264, 201
 Leitherer C., Ferguson H. C., Heckman T. M., Lowenthal J. D., 1995, *Astrophys. J. Lett.*, 454, L19
 López Fernández R., et al., 2018, *A&A*, 615, A27

- Madau P., Pozzetti L., Dickinson M., 1998, *Astrophys. J.*, 498, 106
- Mason C., Trenti M., Treu T., 2015, *Astrophys. J.*, 813, 21
- Mirocha J., Furlanetto S. R., Sun G., 2017, *MNRAS*, 464, 1365
- Morales A. M., Mason C. A., Bruton S., Gronke M., Haardt F., Scarlata C., 2021, *Astrophys. J.*, 919, 120
- Press W. H., Schechter P., 1974, *Astrophys. J.*, 187, 425
- Rees M. J., Ostriker J. P., 1977, *Mon. Not. Roy. Astron. Soc.*, 179, 541
- Reid I. N., Gizis J. E., Hawley S. L., 2002, *Astronomical J.*, 124, 2721
- Robertson B. E., Ellis R. S., Furlanetto S. R., Dunlop J. S., 2015, *Astrophys. J. Lett.*, 802, L19
- Sánchez S. F., et al., 2019, *MNRAS*, 482, 1557
- Serenelli A. M., Fukugita M., 2007, *Astrophys. J. Suppl.*, 172, 649
- Sheth R. K., Tormen G., 1999, *Mon. Not. Roy. Astron. Soc.*, 308, 119
- Silk J., 1977, *Astrophys. J.*, 211, 638
- Sun G., Furlanetto S. R., 2016, *MNRAS*, 460, 417
- Tacchella S., Trenti M., Carollo C. M., 2013, *Astrophys. J. Lett.*, 768, L37
- Tegmark M., Silk J., Blanchard A., 1994, *Astrophys. J.*, 420, 484
- Trenti M., Stiavelli M., Bouwens R. J., Oesch P., Shull J. M., Illingworth G. D., Bradley L. D., Carollo C. M., 2010, *Astrophys. J. Lett.*, 714, L202
- White S. D. M., Frenk C. S., 1991, *Astrophys. J.*, 379, 52
- Wright A. H., et al., 2017, *Mon. Not. Roy. Astron. Soc.*, 470, 283
- Yoshida N., Stoehr F., Springel V., White S. D. M., 2002, *Mon. Not. Roy. Astron. Soc.*, 335, 762